ARTICLES
PUBLISHED ONLINE: 3 OCTOBER 2016 | DOI: 10.1038/NPHOTON.2016.182
nature photonics

An ultrawide-bandwidth single-sideband modulator for terahertz frequencies

A. S. Meijer, G. Berden*, D. D. Arslanov, M. Ozerov, R. T. Jongma and W. J. van der Zande

Wireless high-speed data communication using terahertz (THz) carrier frequencies is becoming reality with data rates beyond 100 Gbit s^{-1}. Many of the mobile applications use internet access and require that THz wireless base stations are connected to a global network, such as the radio-over-fibre network. We present the realization of an ultrawide bandwidth THz optical single-sideband (OSSB) modulator for converting (free-space) THz signals to THz optical modulations with an increased spectral efficiency. THz OSSB will mitigate chromatic dispersion-induced propagation losses in optical fibres and support digital modulation schemes. We demonstrate THz OSSB for free-space radiation between 0.3 and 1.0 THz using a specially designed dichroic beamsplitter for signal and carrier, and a planar light-wave circuit with multimode interference structures. This arrangement of optical elements mimics the Hartley single-sideband modulator for electronics signals and accomplishes the required Hilbert transform without any frequency-dependent tuning element over an ultrawide THz spectrum.

The data rate of our communication systems doubles every 18 months, according to Edholm's law[1]. Social media, virtual reality, high-definition TV, the internet of things and big data all contribute to the expectation that Edholm's law remains valid in the near future. An obvious way for communication technologies to facilitate this growth is to use terahertz (THz) modulation frequencies (0.1–10 THz, 30–3,000 μm)[2–8]. Compact frontend semiconductor devices for THz wireless communication systems are being developed at a rapid pace using the monolithic microwave integrated circuit (MMIC) platform[4,9,10]. MMIC technology combines solid-state receiver and transmitter modules on a single chip with amplifiers and broadband in-phase/quadrature (I/Q) terminals for THz wireless links beyond 100 Gbit s^{-1} (ref. 4).

A challenge of THz wireless communication is the substantial free-space path loss of distant THz sources, and the atmospheric attenuation of free-space radiation with carrier frequencies larger than 100 GHz by water vapour[11] and under weather conditions with rain and fog[12]. A promising solution is the use of the radio-over-fibre (RoF) backbone network[13,14], which at the same time provides direct access to global data servers. THz signals are transported over long distances through low-loss optical fibres and only wirelessly transmitted over the final mile to the end user. Conversion of (free-space) THz signals to THz optical modulations is provided by electro-optical (EO) methods[15,16], which are broadband and have a large dynamic range. EO modulators are able to connect RoF and wireless communication networks seamlessly in terms of carrier frequencies, data rates and I/Q modulation formats. Yet, the major challenges for RoF networks are the large occupied bandwidth in THz EO heterodyning because of the optical double-sideband (ODSB) generation, and the chromatic dispersion-induced propagation losses in analog and digital modulation schemes[13,17]. Optical single-sideband (OSSB) modulators are utilized in RoF networks at megahertz and gigahertz frequencies to mitigate both these effects and to support advanced I/Q modulation formats[18]. In OSSB at THz frequencies, the necessary Hilbert transform between the in-phase and quadrature components (90° phase difference) forms an experimental challenge, especially for broad bandwidth signals. Existing schemes fulfil OSSB only for specific frequencies and inherently operate in the narrowband regime, using techniques such as optical filtering[19,20], time delays as phase shifters in a Sagnac[21,22] or Mach–Zehnder interferometer (MZI)[23], narrowband reflection from fibre Bragg gratings[24,25], stimulated Brillouin scattering in optical fibres[26,27] and a so-called 90° hybrid coupler[28,29].

Here, we present an OSSB modulator that comprises standard optical phase-shifting elements and fibre-optic components in a MZI configuration with EO modulators for the direct conversion of free-space THz radiation. Our modulator accomplishes THz OSSB without any frequency-dependent tuning and provides ultrawide bandwidth operation. This is demonstrated experimentally in the 0.3–1.0 THz range.

Single-sideband (SSB) generation was invented[30] as a refinement of radio modulation for the efficient use of spectral bandwidth and transmission power, and for the mitigation of dispersion-induced propagation losses, also called a 'power penalty'. The efficiency improvement stems from the realization that a single upper sideband (USB) or a single lower sideband (LSB) each contains the complete signal-modulation information. The power penalty originates from the interference of sidebands with the carrier during propagation in dispersive media. In the same spirit, carrier-suppressed OSSB modulation techniques were developed to improve dynamic range[31], to prevent nonlinearities in optical fibres[32], to increase gain of the sideband in an optical amplifier[33] and to increase spectral efficiency[18,20]. Fundamentally, SSB generation is a special case of quadrature modulation and is the interferometric process of a modulation signal and its Hilbert transform, given by[34]:

$$E_{\mathrm{SSB}}(t) = E_{\mathrm{c}}(t)\left(\mathrm{e}^{i\omega_{\mathrm{c}}t + i\delta\sin(\omega_{\mathrm{sig}}t)} \pm i\mathrm{e}^{i\omega_{\mathrm{c}}t + i\delta\cos(\omega_{\mathrm{sig}}t)}\right) \quad (1)$$

where $E_{\mathrm{SSB}}(t)$ is the generated SSB modulation, $E_{\mathrm{c}}(t)$ the carrier electric field, ω_{c} is the carrier frequency and ω_{sig} is the signal frequency. If the modulation depth δ is small, equation (1) can be approximated as:

$$\begin{aligned} E_{\mathrm{SSB}}(t) &= E_{\mathrm{c}}(t)\mathrm{e}^{i\omega_{\mathrm{c}}t}(1 + i\delta\sin(\omega_{\mathrm{sig}}t)) \pm iE_{\mathrm{c}}(t)\mathrm{e}^{i\omega_{\mathrm{c}}t}(1 + i\delta\cos(\omega_{\mathrm{sig}}t)) \\ &= E_{\mathrm{c}}(t)(\mathrm{e}^{i\omega_{\mathrm{c}}t \pm (\pi/2)} \mp 2\delta\mathrm{e}^{i(\omega_{\mathrm{c}} \mp \omega_{\mathrm{sig}})t}) \end{aligned} \quad (2)$$

Institute for Molecules and Materials, FELIX Laboratory, Radboud University, Toernooiveld 7c, Nijmegen 6525 ED, The Netherlands.
*e-mail: g.berden@science.ru.nl

© 2016 Macmillan Publishers Limited, part of Springer Nature. All rights reserved.

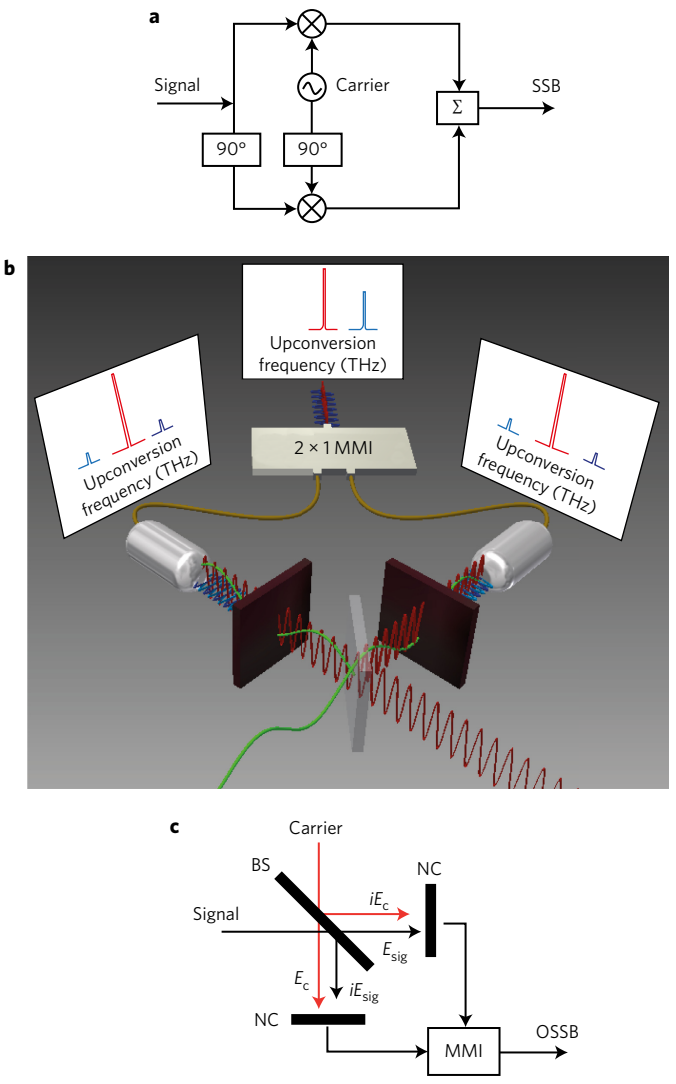

Figure 1 | Experimental scheme for SSB generation. a, Principle of the Hartley modulator for electronic SSB generation with phase shifts for the signal and carrier. **b**, Ultrawideband OSSB generator with two beamsplitter (BS) coatings on a single substrate that ensure the necessary phase shifts to produce signal and carrier beams in quadrature. The NC generate ODSB in quadrature followed by coherent addition in a PLC with MMI structures. The output of the OSSB modulators is demultiplexed and analysed with a high-resolution grating-based spectrometer–CCD combination. **c**, Schematic of the OSSB modulator principle. E_c and E_{sig} are the electric field of the carrier and the signal, respectively.

Equation (2) illustrates that either the USB or the LSB is coherently suppressed. The $\pi/2$ phase difference of the carrier with respect to the SSB ensures orthogonality, which removes the dispersion-induced propagation losses. This interferometric process not only increases the spectral efficiency by suppressing one sideband, but also transfers all the modulation to the one sideband, which leads to a twofold increase of the SSB electric field, and hence a fourfold increase of the SSB intensity. The principle of a Hartley modulator for electronic SSB generation is illustrated in Fig. 1a and has the advantage of being a simple system with a deterministic analytical description given by equations (1) and (2) that provides insight into the generation, propagation and detection of quadrate modulation[30].

Figure 1b depicts our THz OSSB generator using standard optical phase-changing elements in an innovative composition. The beamsplitter combines broadband THz and optical dichroic mirror coatings on a single substrate and has two output ports that are in quadrature, each consisting of a signal and a carrier beam. As it happens, each dichroic beamsplitter coating generates two beams according to $I = T + R + 2RT\cos\theta$, where I is the total intensity of the input beam, R is the intensity of the reflected beam, T the intensity of the transmitted beam and θ represents the phase angle between R and T. $\theta = \pi/2$ when using a 50/50 beamsplitter with a lossless substrate. The two output ports R and T are in quadrature and combine carrier and signal equivalent to the Hartley modulator, as shown in Fig. 1a, but without the need of phase shifters to accomplish the necessary Hilbert transform. In our OSSB set-up, each combination of a carrier beam and a signal beam is mixed in a nonlinear crystal (NC) to generate ODSB modulation. The carrier beam originates from a near-infrared single-mode diode laser and the signal from the far-infrared free-electron laser (FLARE) that delivers short, intense pulses of tunable narrow-bandwidth THz radiation (see Methods). The two ODSB-modulated carrier beams are combined coherently in a planar light wave circuit (PLC) with multimode interference (MMI) structures designed to prevent additional phase changes (see Methods). The interferometric process in the MMI results in OSSB generation without any frequency-dependent tuning over an ultrawide THz bandwidth.

The single-shot ODSB spectrum of each interferometric arm of the OSSB modulator is shown in Fig. 2 for a modulation frequency of 0.69 THz obtained by blocking one of the arms. The observed difference in USB and LSB intensities of the order of 10% is attributed to polarization and spatial filtering effects of the fibre-optic couplers. When the two ODSB signals are combined, interference takes place and OSSB generation can be observed clearly. The ratio of the USB and the LSB changes substantially. In the results shown, the spectral efficiency of OSSB is illustrated by a strong suppression of the LSB intensity, whereas the USB intensity is enhanced by a factor of four, as is expected from equation (2). The inset in Fig. 2 illustrates the ultrawide bandwidth nature of our OSSB modulator and demonstrates OSSB signals for the spectral range between 0.4 and 1 THz.

Even though specific measures to stabilize optical path length differences (OPLDs), like closed environment, temperature and kinematic control, are not implemented in our modulator, seconds of stable OSSB can be readily found, as is shown in Fig. 3a. The visibility of OSSB modulation is defined as $(I_{USB} - I_{LSB})/(I_{USB} + I_{LSB})$, where I_{USB} and I_{LSB} are the integrated peak intensities of the USB and LSB. We observe in Fig. 3a slow drifts from the optimal OSSB signal for the USB to the optimal OSSB signal for the LSB, which indicates that OPLDs occur on the length scale of the carrier wavelength, according to equation (2). This results in either addition or subtraction in the MMI, which is similar to lower or upper OSSB generation. The shot-by-shot ODSB generation in both arms is stable and shows constant visibility. Figure 3b,c depicts the shot-by-shot stability of ODSB generation as a narrow distribution of visibility, which indicates a stable intensity ratio between the USB and LSB signals. When the two interferometric arms are combined, the visibility distribution of Fig. 3d spreads over the complete range of visibility values and peaks at values that agree with OSSB generation. Figure 4 shows the maximum observed visibility at various THz frequencies. Although, in principle, one can achieve infinite suppression of the USB or LSB, imperfections in the beamsplitter and imperfect matched pairs of NCs, optical couplers, fibre lengths and quadrature beam intensities lead to additional phase shifts and therefore a decrease of the visibility and the OSSB dynamic range. At around 0.4 THz, our arrangement of the OSSB modulator shows a maximum visibility of 0.985. The visibility decreases towards lower and higher THz frequencies. Small depolarization perturbations in polarization maintaining (PM) fibres, such as minor stress because of bends and twists, and changes in ambient conditions, affect the

© 2016 Macmillan Publishers Limited, part of Springer Nature. All rights reserved.

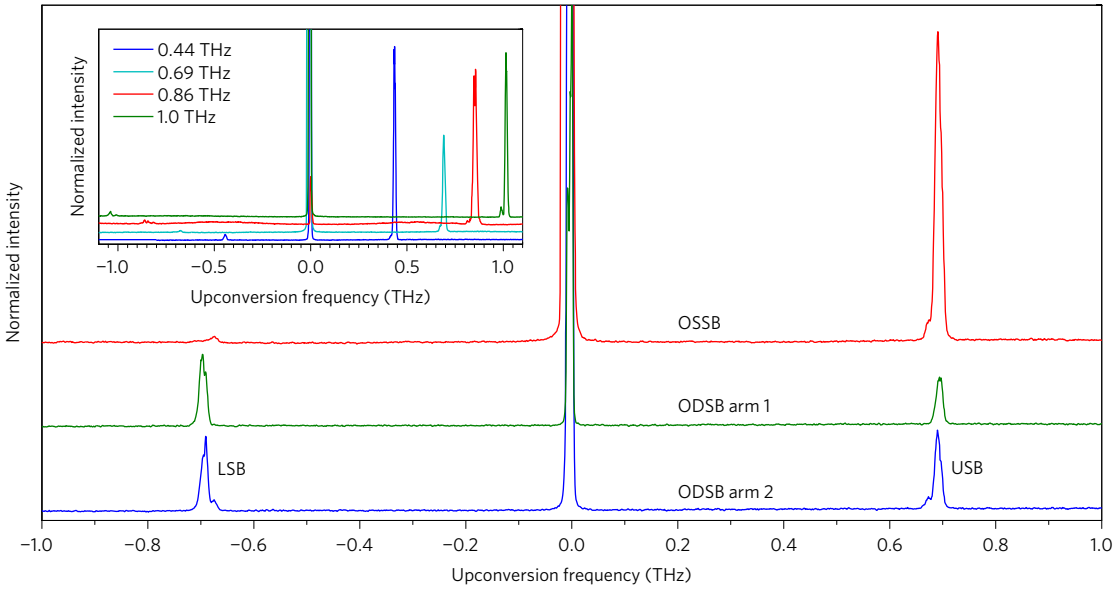

Figure 2 | Single-shot sideband spectra at 0.69 THz. ODSB spectra from each interferometric arm separately and from the interferometric arms combined for OSSB generation. The spectra have been vertically offset for readability. Cross-polarization filtering is used for reduction of the carrier. The inset shows a selection of single-shot traces of OSBB generation at various THz frequencies.

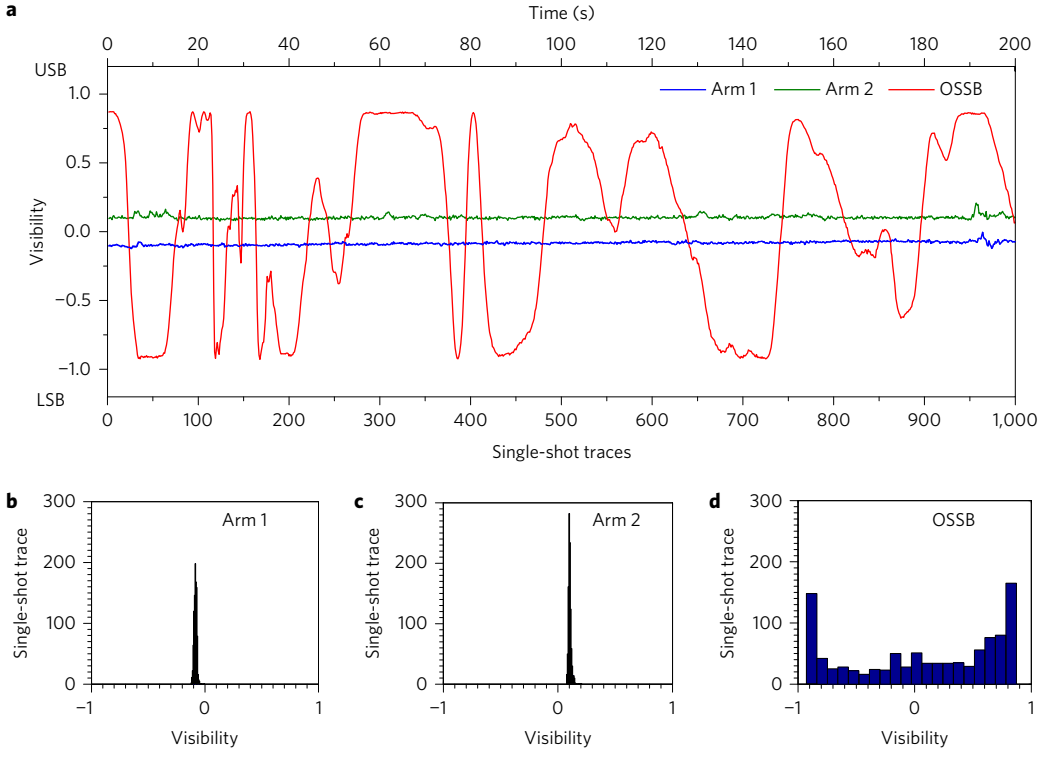

Figure 3 | Visibility measurements. a, Single-shot visibility measurements at 0.62 THz for each interferometric arm separately and for the OSSB generation of the combined interferometric arms. **b–d**, Histograms of the same sets of measurements that show the distributions of single-shot measurements of the visibility for each interferometric arm separately (ODSB) and the interferometric arms combined (OSSB).

carrier suppression by cross-polarization filtering and thereof the OSSB dynamic range. Typical interferometric visibility in classical MZI configurations without active stabilization is approximately −9 dB (ref. 35) and can achieve −20 dB in PLC[36]. In our experimental set-up, we have achieved a visibility of −18 dB for OSSB generation at 0.38 THz.

Given the spectral dependence of the properties of the optical components, like the ZnTe NCs, OSSB generation up to 3 THz should be possible. A next technological step should involve a fully integrated miniaturized THz OSSB modulator using the fibre-optic platform with MMI structures and EO modulators. A compatibility with microdevice platforms[37] will provide interferometric stability and will allow THz OSSB modulators to become economically viable. To enable this compatibility, planar MZI with MMI structures operating at 1,550 nm (ref. 38) should be used with polymer EO modulators to mitigate signal distortion.

© 2016 Macmillan Publishers Limited, part of Springer Nature. All rights reserved.

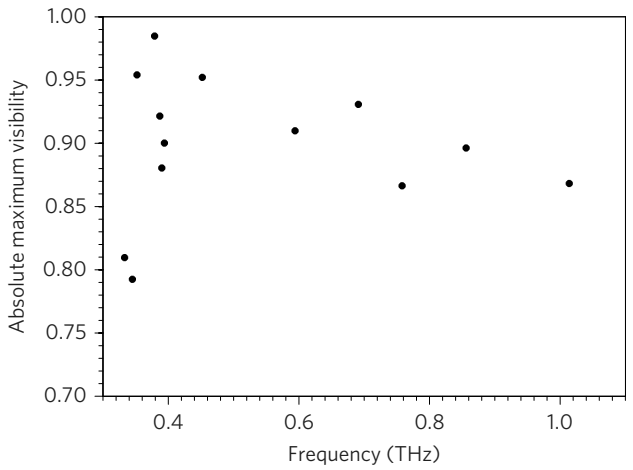

Figure 4 | The maximum observed visibility for OSSB generation at different THz frequencies.

Polymer EO modulators have a gapless frequency response over a wide THz range with nearly flat upconversion efficiency over a 50–100 GHz spectral bandwidth[39]. Also, the chromophores in polymer EO modulators can have nonlinear coefficients one-order larger than those of ZnTe[39,40] and, hence, sideband intensities that are two orders larger. Finally, the collinear EO mixing in our THz OSSB should be replaced by patch antenna-coupled EO modulators[41–43]. Confinement of focused THz electric fields (square millimetres) to the lateral dimensions of planar waveguides (square micrometres) by resonant patch antenna structures can significantly enhance the upconversion efficiency[44–46].

In conclusion, we realized an ultrawide bandwidth OSSB modulator for the direct conversion of free-space THz electromagnetic radiation to THz optical modulations. Specially designed dichroic beamsplitter coatings for signal and carrier on a single substrate create two output ports in quadrature, each consisting of a carrier and signal, and accomplishes the necessary Hilbert transform in OSSB. Another vital element is the PLC–MMI, which allows interferometric recombination of beams over an ultrawide THz bandwidth without additional phase changes. Carrier suppression by cross-polarization filtering increases the OSSB dynamic range and a sideband suppression ratio of −18 dB is achieved. THz OSSB generation can be used to mitigate the chromatic dispersion-induced propagation losses in RoF networks, to increase spectral efficiency and to support I/Q modulation formats. Future miniaturization may involve patch antenna-coupled EO geometries in MZI configurations for compatibility with the microdevice platform. Our general OSSB method can be seen as a stepping stone towards optical data communication at THz frequencies.

Methods

Methods and any associated references are available in the online version of the paper.

Received 17 May 2016; accepted 15 August 2016; published online 3 October 2016

References

1. Cherry, S. Edholm's law of bandwidth. *IEEE Spectrum* **41,** 58–60 (2004).
2. Tonouchi, M. Cutting-edge terahertz technology. *Nat. Photon.* **1,** 97–105 (2007).
3. Federici, J. & Moeller, L. Review of terahertz and subterahertz wireless communications. *J. Appl. Phys.* **107,** 111101 (2010).
4. Koenig, S. *et al.* Wireless sub-THz communication system with high data rate. *Nat. Photon.* **7,** 977–981 (2010).
5. Akyildiz, I. F., Jornet, J. M. & Han, C. Terahertz band: next frontier for wireless communications. *Phys. Commun.* **12,** 16–32 (2014).
6. Karl, N. J., McKinney, R. W., Monnai, Y., Mendis, R. & Mittleman, D. M. Frequency-division multiplexing in the terahertz range using a leaky-wave antenna. *Nat. Photon.* **9,** 717–720 (2015).
7. Ferguson, B. & Zhang, X.-C. Materials for terahertz science and technology. *Nat. Mater.* **1,** 26–33 (2002).
8. Yoshimizu, Y. *et al.* Generation of coherent sub-terahertz carrier with phase stabilization for wireless communications. *J. Commun. Netw.* **15,** 569–575 (2013).
9. Song, H., Tajima, T., Yaita, M. & Kagami, O. Recent progress in terahertz MMICs and packages for terahertz wireless communications at 300 GHz. In *39th Int. Conf. Infrared, Millimeter, and Terahertz Waves* (eds Siegel, P. H. & Walker, C.) 1–1 (IEEE, 2014).
10. Kallfass, I. *et al.* MMIC chipset for 300 GHz indoor wireless communication. In *Int. Conf. Microwaves, Communications, Antennas and Electronic Systems* (eds Auster, S. & Boag, A.) 1–4 (IEEE, 2015).
11. Yang, Y., Shutler, A. & Grischkowsky, D. Measurement of the transmission of the atmosphere from 0.2 to 2 THz. *Opt. Express* **19,** 8830–8838 (2011).
12. Huang, K.-C. & Wang, Z. Terahertz terabit wireless communication. *IEEE Microw. Mag.* **12,** 108–116 (2011).
13. Beas, J., Castanon, G., Aldaya, I., Aragón-Zavala, A. & Campuzano, G. Millimeter-wave frequency radio over fiber systems: a survey. *IEEE Commun. Surv. Tut.* **15,** 1593–1619 (2013).
14. Alavi, S. E. *et al.* Towards 5G: a photonic based millimeter wave signal generation for applying in 5G access fronthaul. *Sci. Rep.* **6,** 19891 (2016).
15. Wu, Q. & Zhang, X.-C. Ultrafast electro-optic field sensors. *Appl. Phys. Lett.* **68,** 1604–1606 (1996).
16. Sinyukov, A. M. & Hayden, L. M. Efficient electrooptic polymers for THz applications. *J. Phys. Chem. B* **108,** 8515–8522 (2004).
17. Smith, G. H. & Novak, D. Broad-band millimeter-wave (38 GHz) fiber-wireless transmission system using electrical and optical SSB modulation to overcome dispersion effects. *IEEE Photon. Technol. Lett.* **10,** 141–143 (1998).
18. Kitayama, K. Highly spectrum efficient OFDM/PDM wireless networks by using optical SSB modulation. *J. Lightwave Technol.* **15,** 969–976 (1998).
19. Lu, H. H., Tzeng, S. J., Chen, C. Y. & Peng, H. C. CSO/CTB performances improvement by using optical SSB filter at the receiving site. *IEEE Trans. Commun.* **53,** 752–575 (2005).
20. Xiao, S. & Weiner, A. M. Optical carrier-suppressed single sideband (O-CS-SSB) modulation using a hyperfine blocking filter based on a virtually imaged phased-array (VIPA). *IEEE Photon. Techn. Lett.* **17,** 1522–1524 (2005).
21. Li, F. & Helmy, A. S. Gigahertz to terahertz tunable all-optical single-side-band microwave generation via semiconductor optical amplifier gain engineering. *Opt. Lett.* **38,** 4542–4545 (2013).
22. Zheng, J. *et al.* Orthogonal single-sideband signal generation using improved Sagnac-loop-based modulator. *IEEE Photon. Technol. Lett.* **26,** 2229–2231 (2014).
23. Smith, G. H., Novak, D. & Ahmed, Z. Technique for optical SSB generation to overcome dispersion penalties in fibre-radio systems. *Electron. Lett.* **33,** 74–75 (1997).
24. Burla, M. *et al.* Integrated waveguide Bragg gratings for microwave photonics signal processing. *Opt. Express* **21,** 25120–25147 (2013).
25. Sima, C. *et al.* Terahertz bandwidth photonic Hilbert transformers based on synthesized planar Bragg grating fabrication. *Opt. Express* **38,** 3448–3451 (2013).
26. Sagues, M. & Loayssa, A. Orthogonally polarized optical single sideband modulation for microwave photonics processing using stimulated Brillouin scattering. *Opt. Express* **18,** 22906–22914 (2010).
27. Zhen'ao, L., Liang, X., Xiaoqiong, Q. & Hui, W. 30-GHz millimeter-wave carrier generation with single sideband modulation based on stimulated Brillouin scattering. *J. Semicond.* **33,** 092004 (2011).
28. Campillo, A. L. Orthogonally polarized single sideband modulator. *Opt. Lett.* **32,** 3152–3154 (2007).
29. Wang, W. T., Liu, J. G., Mei, H. K. & Zhu, N. H. Phase-coherent orthogonally polarized optical single sideband modulation with arbitrarily tunable optical carrier-to-sideband ratio. *Opt. Express* **24,** 388–399 (2016).
30. Hartley, R. V. Transmission of information. *Bell Syst. Tech. J.* **7,** 535–563 (1928).
31. Esman, R. D. & Williams, K. J. Wideband efficiency improvement of fiber optic systems by carrier subtraction. *IEEE Photon. Technol. Lett.* **7,** 218–220 (1995).
32. Yang, F. S., Marhic, M. E. & Kazovsky, L. G. Nonlinear crosstalk and two countermeasures in SCM-WDM optical communication systems. *J. Lightwave Technol.* **18,** 512–520 (2000).
33. Jansen, S., Morita, I. & Tanaka, H. Carrier-to-signal power ratio in fiber-optic SSB-OFDM transmission systems. In *Inst. Electronics, Information and Communication Engineers Gen. Conf.* B-10–24, 363 (Institute of Electronics, Information and Communication Engineers, 2007).
34. Carlson, A. B., Crilly, P. B. & Rutledge, J. C. *Communication Systems: an Introduction to Signals and Noise in Electrical Communication* 167–169 (McGraw-Hill, 1986).
35. Rao, D. N. & Kumar, V. N. Stability improvements for an interferometer through study of spectral interference patterns. *Appl. Opt.* **38,** 2014–2017 (1999).

© 2016 Macmillan Publishers Limited, part of Springer Nature. All rights reserved.

36. Schnarrenberger, M., Zimmermann, L., Mitze, T., Bruns, J. & Petermann, K. Mach–Zehnder interferometer (MZI) with more than 20 dB extinction ratio on silicon-on-insulator. In *2nd IEEE Int. Conf. Group IV Photonics* 132–133 (IEEE, 2005).
37. Jazbinsek, M., Mutter, L. & Günter, P. Photonic applications with the organic nonlinear optical crystal DAST. *IEEE J. Sel. Top. Quantum Electron.* **14,** 1298–1311 (2008).
38. Han, J., Seo, B. J., Han, Y., Jalali, B. & Fetterman, H. R. Reduction of fiber chromatic dispersion effects in fiber-wireless and photonic time-stretching system using polymer modulators. *J. Lightwave Technol.* **21,** 1504–1509 (2003).
39. McLaughlin, C. V. *et al.* Wideband 15 THz response using organic electro-optic polymer emitter-sensor pairs at telecommunication wavelengths. *Appl. Phys. Lett.* **92,** 151107 (2008).
40. Kim, T.-D. *et al.* Ultralarge and thermally stable electro-optic activities from supramolecular self-assembled molecular glasses. *J. Am. Chem. Soc.* **129,** 488–489 (2007).
41. Wijayanto, Y. N., Murata, H. & Okamura, Y. Electro-optic wireless millimeter-wave-lightwave signal converters using planar Yagi–Uda array antennas coupled to resonant electrodes. In *Proc. 17th Opto-Electronic Communications Conf.* (eds Kim, C.-M. & Chung, Y. C.) 5E1–2 (IEEE, 2012).
42. Salamin, Y. *et al.* Direct conversion of free space millimeter waves to optical domain by plasmonic modulator antenna. *Nano Lett.* **15,** 8342–8346 (2015).
43. Zhang, X. *et al.* Integrated broadband bowtie antenna on transparent silica substrate. *IEEE Antennas Wirel. Propag. Lett.* **15,** 1377–1381 (2016).
44. Seo, M. A. *et al.* Terahertz field enhancement by a metallic nanoslit operating beyond the skin-depth limit. *Nat. Photon.* **3,** 152–156 (2009).
45. Novitsky, A., Zalkovskij, M., Malureanu, R., Jepsen, P. U. & Lavrinenko, A. V. Optical waveguide mode control by nanoslit-enhanced terahertz field. *Opt. Lett.* **37,** 3903–3905 (2012).
46. Park, S. J. *et al.* Detection of microorganisms using terahertz metamaterials. *Sci. Rep.* **4,** 4988 (2014).

Acknowledgements

This work is part of the research programme of the Foundation for Fundamental Research on Matter (FOM), which is part of the Netherlands Organization for Scientific Research (NWO). FLARE is funded via the 'Big Facilities' programme of NWO. The authors gratefully thank the FELIX laboratory staff for their skilled support and A. Kimel for fruitful discussions.

Author contributions

A.S.M., G.B. and W.J.Z. conceived and designed the experiments. A.S.M. built the experimental set-up and performed all the measurements. D.D.A., M.O. and R.T.J. operated the THz free-electron laser (FLARE), the FLARE diagnostic tools and the upconversion spectrometer. A.S.M., R.T.J. and W.J.Z. analysed the experimental data. A.S.M. and W.J.Z. wrote the manuscript with contributions from G.B. and R.T.J.

Additional information

Reprints and permissions information is available online at www.nature.com/reprints. Correspondence and requests for materials should be addressed to G.B.

Competing financial interests

The authors declare no competing financial interests.

© 2016 Macmillan Publishers Limited, part of Springer Nature. All rights reserved.

Methods

The ultrawideband OSSB modulator of Fig. 1b,c is realized experimentally using a frequency-stabilized 1 W continuous wave (CW) 780 nm laser (Toptica DL-100 with a frequency-stabilization module) as carrier. The required THz signal is provided by the free-electron laser FLARE[47], part of the Free Electron Lasers for Infrared eXperiments (FELIX) Laboratory at the Radboud University in Nijmegen, operating in the frequency range 0.3–1.0 THz (bandwidth approximately 0.5% of the frequency). The pulse structure of FLARE consists of macropulses and micropulses. The macropulses have a repetition frequency of 5 Hz and a pulse duration of 5 μs. Each macropulse consists of a 3 GHz train of Fourier-transform limited micropulses of 42–140 ps duration with pulse energies of 0.7–4.0 μJ.

The specially designed 50/50 beamsplitter is devised from a double-side polished quartz glass of 1 ± 0.1 mm thick (80–50 scratch-dig) with an indium tin oxide (ITO) coating ($20 \pm 5\ \Omega\ sq^{-1}$ (Praezisions Glass & Optik)). In the range 0.3–1.0 THz, the absorption in quartz[48] is ~1% and ITO is assumed to be lossless[49]. The ITO coating is estimated to be larger than 150 nm and has a reflectivity of 85% at 45° incident. A 50/50 beam THz beamsplitter is obtained by etching the ITO coating and decreasing the ITO coating thickness. The ITO etch rate of 2 nm min^{-1} in hydrochloric acid (1:1 HCL:H_2O) is determined empirically. Monitoring the THz electric field transmission with a THz time-domain spectrometer (TERA K15, Menlo Systems), the ITO coating thickness is etched to 45 ± 8 nm (NT1100, Wyko) for 50/50 beam splitting, which is in good agreement with a skin depth of ~300 nm (ref. 49). A large variation in ITO thickness is caused by inhomogeneous etching. On the opposite side of the quartz glass, a 780 nm nonpolarizing dielectric beamsplitter coating is deposited for a 45° incident radiation (Laseroptik). Each output port of the beamsplitter consists of a carrier and a signal, which are mixed in a 1 mm thick <110> ZnTe crystal. This modulation of the carrier by the THz electric field in the NC generates phase-coherent ODSB[50–52]. For narrowband upconversion, the energy of the sidebands scales linearly with the carrier power and THz energy[51]. For the present set-up, the conversion efficiency, which is defined as the ratio of the sideband and THz energy, is about 10^{-9} for a 10 mW CW carrier power[51]. The two resulting ODSB beams are coupled in two fibres and coherently combined in the 2 × 1 MMI combiner (XioPhotonics). The central structure of a MMI device is a waveguide resonator designed to support a large number of modes. A number of single-mode access waveguides are used to launch light selectively into the MMI structure and to recover light selectively from the MMI structure. The operation area of the MMI supports bandwidths as large as 20 nm. The interferometric arms in Fig. 1b have lengths of 30 mm from the beamsplitter to the fibre couplers and 1 m of PM optical fibres towards the MMI structure. The output of the MMI is inspected with a spectrometer–CCD (charge-coupled device) set-up, which consists of a 1.5 m focal length high-resolution grating-based spectrometer (Jobin Yvon THR1500) and a 3,600 pixel linear CCD array (Alphalas S3600-D with a Toshiba TCD1304 sensor).

The polarization directions of the carrier and the THz radiation are parallel, which maximizes ODSB generation[51,52]. The ODSB components are orthogonally polarized with respect to the carrier. We use this orthogonality to increase the OSSB dynamic range by carrier suppression with cross-polarization filtering[51,53] between the exit of the MMI combiner and the grating spectrometer. The high instantaneous THz power of FLARE enables effective mixing with a CW carrier laser[51]. The spectrometer–CCD combination is sensitive enough to record the generated OSSB by a single THz macropulse, which relaxes the demands on the mechanical stability of the set-up considerably. Our balanced MZI is stable for the duration of a single macropulse of FLARE.

References

47. Zhaunerchyk, V., Oepts, D., Jongma, R. T. & van der Zande, W. J. Influence of waveguide dispersion on short-pulse free electron laser detuning curves. *Phys. Rev. ST Accel. Beams* **15,** 050701 (2012).
48. Grischkowsky, D., Keiding, S., Van Exter, M. & Fattinger, C. Far-infrared time-domain spectroscopy with terahertz beams of dielectrics and semiconductors. *J. Opt. Soc. Am. B* **7,** 2006–2015 (1990).
49. Bauer, T., Kolb, J. S., Loffler, T., Mohler, E. & Roskos, H. G. Indium–tin–oxide-coated glass as dichroic mirror for far-infrared electromagnetic radiation. *J. Appl. Phys.* **92,** 2210–2212 (2002).
50. Gallot, G. & Grischkowsky, D. Electro-optic detection of terahertz radiation. *J. Opt. Soc. Am. B* **16,** 1204–1212 (1999).
51. Wijnen, F. J., Berden, G. & Jongma, R. T. A simple optical spectral calibration technique for pulsed THz sources. *Opt. Express* **18,** 26517–26524 (2010).
52. Jamison, S. P., Berden, G., Phillips, P. J., Gillespie, W. A. & MacLeod, A. M. Upconversion of a relativistic Coulomb field terahertz pulse to the near infrared. *Appl. Phys. Lett.* **23,** 231114 (2010).
53. Berden, G. *et al.* Benchmarking of electro-optic monitors for femtosecond electron bunches. *Phys. Rev. Lett.* **99,** 164801 (2007).

© 2016 Macmillan Publishers Limited, part of Springer Nature. All rights reserved.